SANDIA REPORT
SAND97-0675 • UC-706
Unlimited Release
Printed March 1997

Fusion of Radar Data to Extract 3-Dimensional Objects LDRD Final Report

Rick Fellerhoff, Bill Hensley, Richard Carande, Grant Burkhart, Robert Ledner

Prepared by
Sandia National Laboratories
Albuquerque, New Mexico 87185 and Livermore, California 94550

Sandia is a multiprogram laboratory operated by Sandia Corporation, a Lockheed Martin Company, for the United States Department of Energy under Contract DE-AC04-94AL85000.

Approved for public release; distribution is unlimited.

Sandia National Laboratories

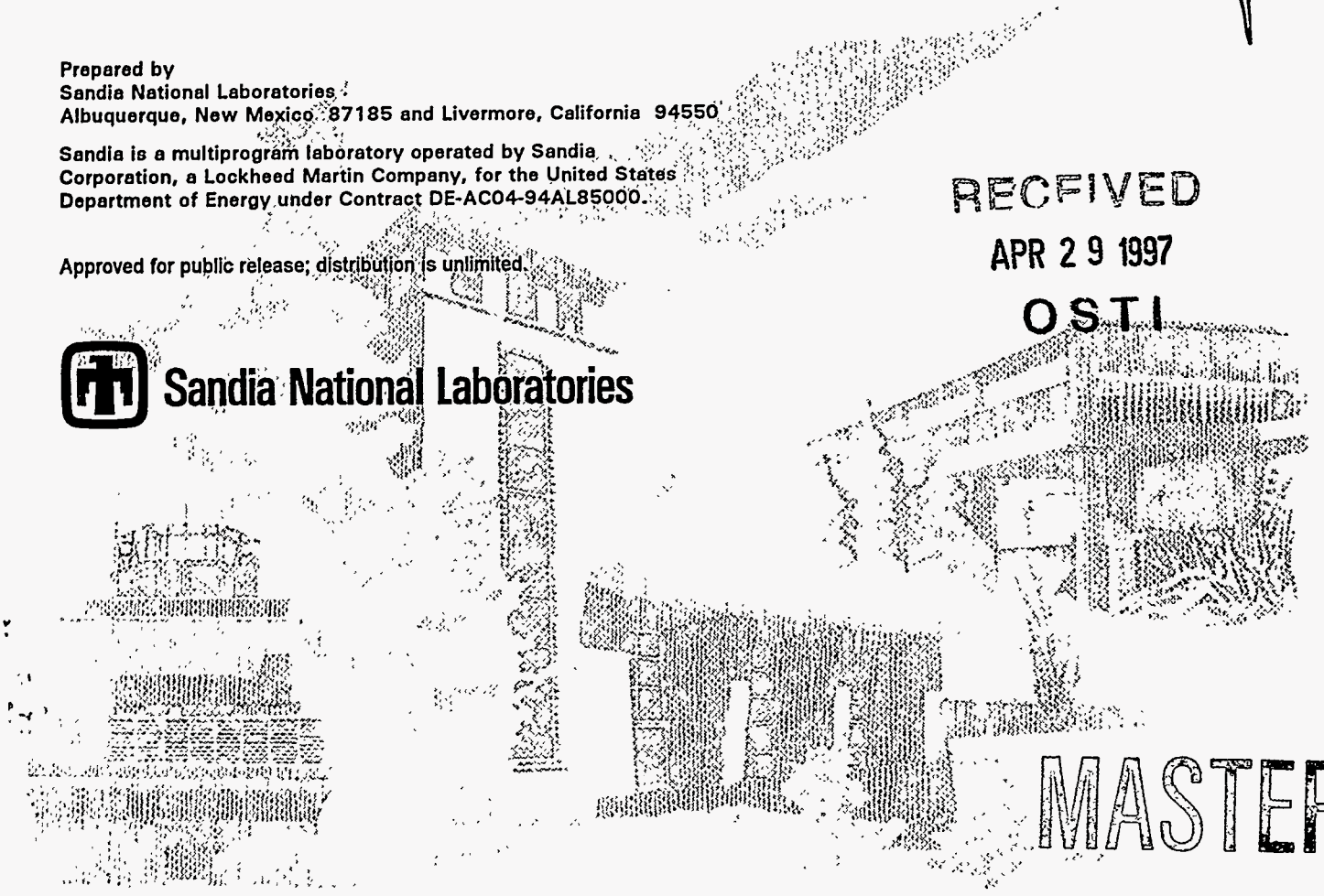

Issued by Sandia National Laboratories, operated for the United States Department of Energy by Sandia Corporation.

Available to DOE and DOE contractors from
Office of Scientific and Technical Information
P.O. Box 62
Oak Ridge, TN 37831

Prices available from (615) 576-8401, FTS 626-8401

Available to the public from
National Technical Information Service
U.S. Department of Commerce
5285 Port Royal Rd
Springfield, VA 22161

NTIS price codes
Printed copy: A03
Microfiche copy: A01

SAND97-0675
Unlimited Release
Printed March 1997

Distribution
Category UC-706

Fusion of Radar Data to Extract 3-Dimensional Objects LDRD Final Report

Rick Fellerhoff
Aided Navigation and Remote Sensing Department

Bill Hensley
Radar Analysis Department

Sandia National Laboratories
P.O. Box 5800
Albuquerque, NM 87185-0843

Richard Carande, Grant Burkhart, Robert Ledner
Vexcel Corporation
2477 55th street
Boulder, CO 80301

Abstract

Interferometric Synthetic Aperture Radar (IFSAR) is a very promising technology for remote mapping of 3-Dimensional objects. In particular, 3-D maps of urban areas are extremely important to a wide variety of users, both civilian and military. However, 3-D maps produced by traditional optical stereo (stereogrammetry) techniques can be quite expensive to obtain, and accurate urban maps can only be obtained with a large amount of human-intensive interpretation work.

IFSAR has evolved over the last decade as a mapping technology that promises to eliminate much of the human-intensive work in producing elevation maps. However, IFSAR systems have only been robustly demonstrated in non-urban areas, and have not traditionally been able to produce data with enough detail to be of general use in urban areas. Sandia Laboratories' Twin Otter IFSAR (Bickel and Hensley, 1996) was the first mapping radar system with the proper parameter set to provide sufficiently detailed information in a large number of urban areas.

The goal of this LDRD was to fuse previously unused information derived from IFSAR data in urban areas that can be used to extract accurate digital elevation models (DEMs) over wide areas without intensive human interaction.

1. Introduction

1.1. History - Problem Statement

Maps of urban areas are extremely important to a wide variety of users, both civilian and military. However, they are traditionally expensive to obtain. Even with mature optical stereo (stereogrammetry) techniques, accurate urban maps can only be obtained with a large amount of human-intensive interpretation work.

A mapping radar technique called interferometric synthetic aperture radar (IFSAR) has evolved over the last decade which eliminates much of the human-intensive work in producing elevation maps in non-urban areas. These systems have not traditionally been able to produce data with enough detail to be of general use in urban areas. Sandia Laboratories' Twin Otter IFSAR (Bickel and Hensley, 1996) was the first mapping radar system with the proper parameter set to provide interpretable height information in a large number of urban areas.

"Interpretable" is a key word, however. Interferometric synthetic aperture radar depends on the phase difference between the complex signals returned from an object on the ground to two antennas offset slightly from each other. The phase difference is readily predictable and interpretable from simple target models in most non-urban areas. One of the key reasons for this is that there is only one object in any given range-doppler cell of the radar image. That is, the mapping from the Earth's surface to the radar imaging plane is one-to-one. This assumption is grossly violated in urban areas.[1] The side of each building roof which is nearest the radar gets superimposed (laid-over in radar parlance) on the ground in front of the building. The IFSAR then measures a weighted average height rather than the correct height for either object. The exact measured height depends on the relative strength of the returns from the roof and the ground. There are also complex scatterers in an urban scene which give extremely good height measurements of such things as the building-to-ground interface height. These features produce an elevation model which is, at first, quite confusing to an interpreter.

The exact implementation of Sandia Laboratories' IFSAR provides information in addition to radar data which gives a variety of clues that these phenomena are occurring. Therefore, we believed it was possible to fuse the available information and detect the effects and predict the correct heights of both the building and the ground. We knew if this was possible, it would greatly enhance the usability of such elevation models for a wide variety of users.

1.2. Project Overview

To quickly get an answer to the question, we teamed up with radar and mapping experts at Vexcel Corporation – a mapping research company in Boulder, Colorado. The Vexcel team consisted of Richard Carande, Grant Burkhart, and Robert Ledner. They have experience in radar mapping, algorithm development, and stereogrammetry, and so are able to rapidly identify common features between elevation models from various data sets and develop fusion algorithms to exploit the unusual characteristics of any given data type.

---

[1] The assumption is also somewhat violated in forested areas – especially when using low radar frequencies. The ambiguities seen when mapping vegetation is another aspect of this same characteristic.

Together, the Sandia and Vexcel teams planned and executed several experiments to collect and produce appropriate data sets. Vexcel produced a highly accurate elevation model from airborne stereo photography which included buildings and trees over three square kilometers of area including Sandia's Technical Area I. This optical DEM was used as ground truth to benchmark the performance of the algorithms developed for the IFSAR data.

The Sandia IFSAR team flew ten flight lines and processed the data into elevation models. The IFSAR models were collected at two urban areas with quite different characteristics. The first area (the "infirmary site") is probably best characterized as suburban. There are a few main buildings in this scene, with a large amount of grass, trees, and roadways in between. Some of the trees in this area are very large – taller than four-story buildings. We produced one elevation model in this area. The second site (the "Building 891" site) covers a portion of Technical Area I which is very densely built-up. It is representative of a heavily-industrialized urban area – although the highest buildings are only 5 floors, shorter than those in the most highly urbanized areas. The "Building 891" site has only a few, relatively small, trees.

The data sets were produced using Sandia's Twin Otter IFSAR processor. This processor produces four outputs for each data point in a model. Besides the elevation at each point, the outputs include the coherence or normalized correlation, the back-scatter intensity, and the bin count. The coherence provides a confidence indicator for each measurement. In urban areas it tends to be of much different character than would normally be expected.. The intensity reflects the return power in each cell. In layover areas the power tends to increase because scattered power from all of the objects which are laid-over into the same cell adds together. The bin count output is unique to Sandia's system. It is a very localized indicator of the incidence angle of the measured surface. (For a more detailed explanation of these outputs, see Bickel and Hensley, 1996)

Vexcel's team then took Sandia's IFSAR data and developed algorithms to detect the phenomena and make predictions of the actual height of both the building roof and the ground in front of the building. The following discussion is a technical description of the work performed by Vexcel for Sandia.

2. Technical Overview

The goal of this project was to exploit previously unused information derived from radar data that can be used to improve digital elevation models (DEM) produced from interferometric synthetic aperture radar (IFSAR). We obtained data from two different sites at Sandia National Laboratory: the *infirmary site* and the *building-894* site. The data that we could use for the two sites included (1) the *backscattered power*, (2) the IFSAR *elevation* in meters from sea level (3) the *binning number* and (4) the *maximum correlation*. The binning number and *maximum correlation* arise from the rectification of the power and elevation. The data are originally processed into range and azimuth, but for rectification the range and azimuth data are transformed into the horizontal coordinate system. This transformation is accomplished with the use of the IFSAR elevation. Since the range and azimuth data do not transform uniformly to the horizontal coordinate system (because of differing elevations), the data are collected into uniformly spaced bins. The binning number is the number of range-azimuth measurements that fall into a bin normalized to the average. The binning number gives additional information: Regions of rising elevation have a smaller binning number and regions of decreasing elevation have larger binning number. As we shall see, the binning number can be very helpful, particularly for the removal of front-porch anomalies. In Figure 1 we show the four types of images for the B-894 site, while in Figure 2 we show the Infirmary site.

Although many measurements fall into a give bin, the final elevation assigned to that bin is taken from only one measurement, the measurement with the greatest correlation. If s_1 and s_2 are the complex signals received by each of the antennas, the correlation is $\frac{s_1 s_2^*}{|s_1||s_2|}$. The maximum correlation is the greatest correlation of the measurements to fall in a bin.

Our work with DEM reconstruction follows four approaches. The first approach is image filtering; the second, tree recognition and extraction; the third, building recognition and extraction, and the fourth is building model construction and DEM reconstruction using the building models and the "bare-earth" DEM.

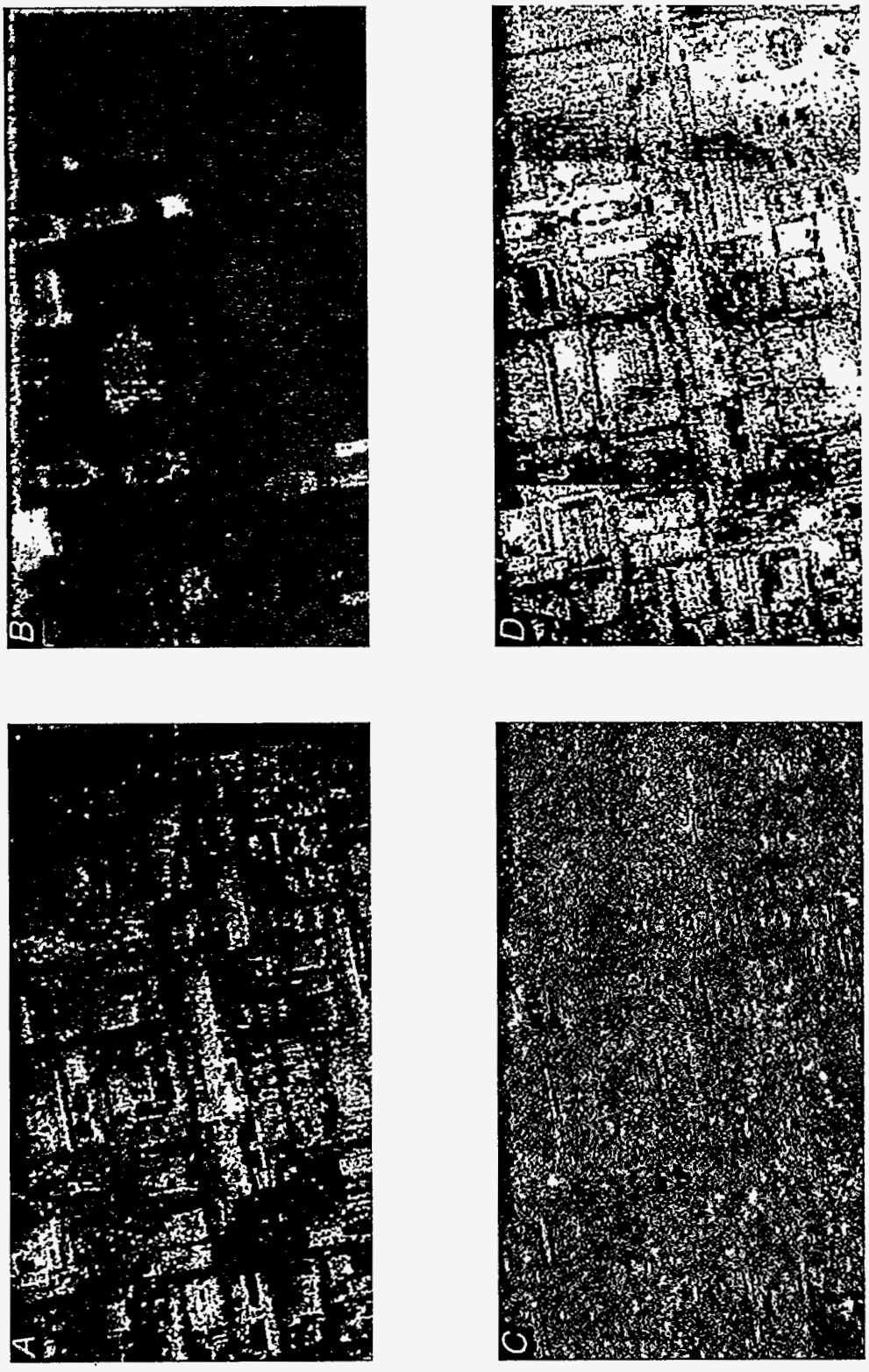

Figure 1: A) The backscattered power, B) elevation, C) binning number and D) maximum correlation for the B-894 site.

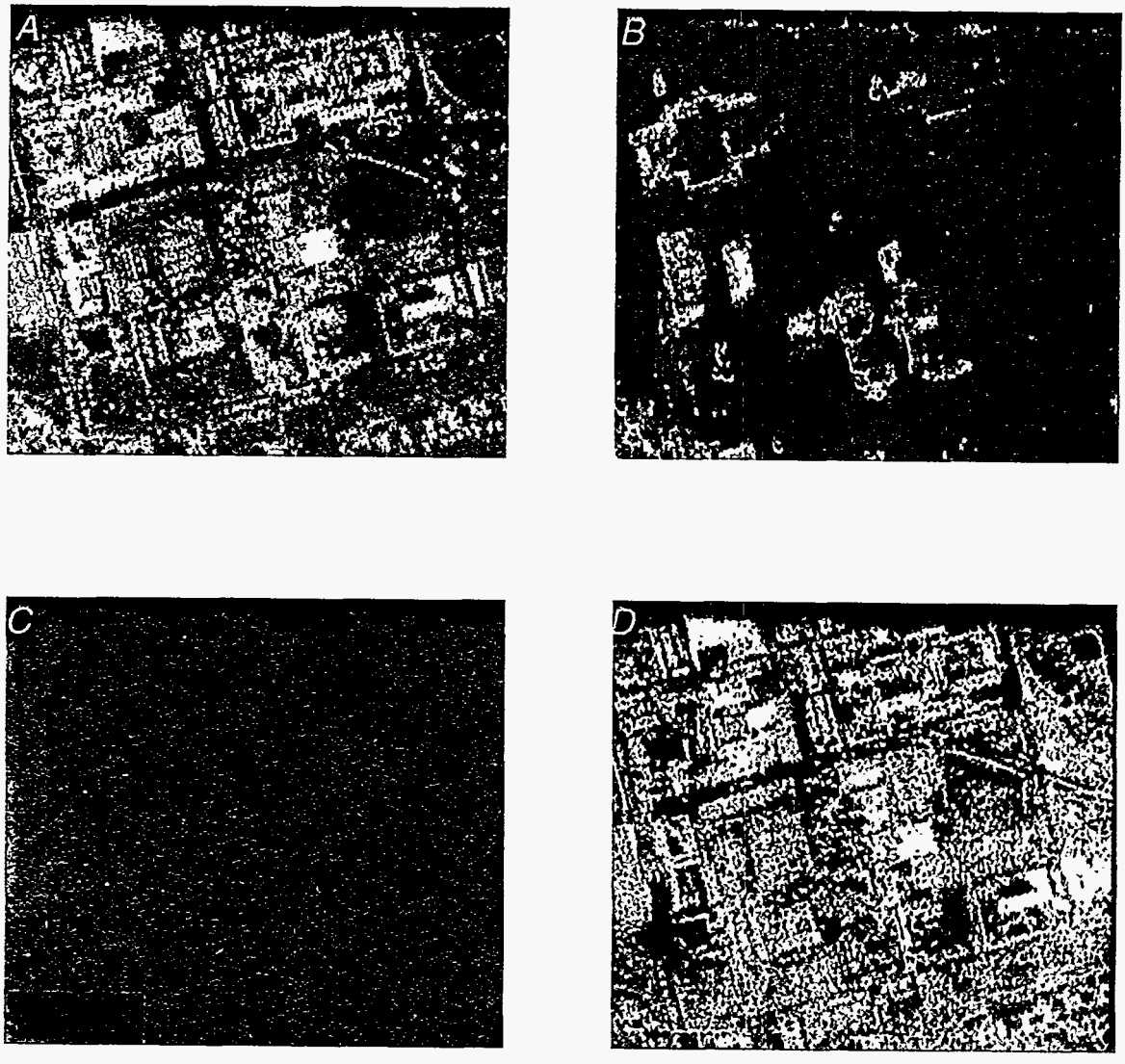

Figure 2: A) The backscattered power, B) elevation, C) binning number and D) maximum correlation for the Infirmary site.

3. Shadow Removal

The first step, before considering either trees or buildings, is to remove shadows. At present, we are considering shadows to be regions where the maximum correlation is less than 0.8. We assume that shadows lie immediately behind a sharp, downward gradient (where behind refers to the direction away from the radar). Although we have no valid information on the elevation in the shadow region, we assume that the elevation within the shadow is *different* from the elevation in front of the shadow. We therefore iteratively extend the elevation into the shadow unless we find that we are extending the elevation along the radar viewing direction. Iteration proceeds until all shadow regions are filled in. This procedure is simple and only in error in the case of noisy data originating from in front of a high region, in which case the noisy region is filled in by the higher elevation. Because this situation is rare, we do not view this as a significant problem.

4. Image Filtering

The next step in the DEM improvement is noise reduction through digital filtering. Essentially, the idea with digital filtering is that noise scale lengths are typically smaller than scale lengths of real features. Application of the filter alters the signal at small scales leaving the large scales intact. Any features on the noise scale are always destroyed by the filter.

A linear filter, such as a box-car average or a Gaussian filter smoothes out all gradients to the noise scale. For the present application, this would alter the vertical building walls to more gentle slopes, so these filters are unacceptable. A median filter has the advantage that building edges stay vertical, however, building edges can move by a distance $l/2$ where l is the filter width.

4.1. Context-Sensitive Diffusion

We define $h_{l,m}$ as the elevation at pixel (l, m), such that the filter,

$$h^{*}_{l,m} = h_{l,m} + D(h_{l+1,m} + h_{l-1,m} + h_{l,m+1} + h_{l,m-1} - 4h_{l,m}),$$

is the discrete form of the diffusion equation

$$\frac{\partial h}{\partial t} = D\nabla^2 h.$$

If a highly localized initial signal, $h = \delta(\mathbf{x})$ is used in equation [2], after a time t

$$h = \left(\frac{1}{4\pi Dt}\right)^{1/2} e^{\frac{x^2}{Dt}}.$$

Thus n applications of the filter [1] is equivalent to a single convolution with the Gaussian Filter

$$f = \left(\frac{1}{4\pi nD}\right)^{1/2} e^{\frac{x^2}{nD}}.$$

For stability, D should be smaller than 1/4. n iterations of [1] results in the removal of noise on length scales less than $(nD)^{1/2}$.

It has been recognized that equation [1] can be modified to include a spatially dependent diffusion coefficient D, thereby allowing for different noise scales in different places. An example is a diffusion coefficient $D = c/|g|$, where c is a constant and $\mathbf{g}$ is the gradient. This allows the beginnings of context sensitivity; where the gradient is large, the filter width $(nD)^{1/2}$ is small and where the gradient is small the filter width is large.

We have modified this method to a true multi-length scale method: A feature edge is identified by its persistence across length scales. In regions far from a feature edge, the diffusion is large while near a feature edge the diffusion is small. Thus, noise is removed to the greatest extent possible, but at the same time the position and abruptness of feature edges is preserved.

Consider the vector gradient $\mathbf{g}_l$, where $g_{x,l} = h_{i+l,j} - h_{i-l,j}$ and $g_{y,l} = h_{i,j+l} - h_{i,j+l}$.. The length-scale-average gradient is $\langle \mathbf{g} \rangle = \left(\frac{1}{l_{\max}} \right) \sum_{l=1}^{l=l_{\max}} \mathbf{g}_l$. This gives the gradient that is consistently present across different length scales. The anisotropic diffusion coefficient is now a tensor:

$$\mathbf{D} = c \frac{\langle \mathbf{gg} \rangle - \langle \mathbf{g} \rangle \langle \mathbf{g} \rangle}{\langle \mathbf{g} \rangle \langle \mathbf{g} \rangle}$$

and the diffusion equation is

$$\frac{\partial h}{\partial t} = \nabla \bullet \mathbf{D} \bullet \nabla h.$$

Consider for example

$$D_{xx} = c \frac{\langle g_x^2 \rangle - \langle g_x \rangle^2}{\langle g_x \rangle^2}$$

If the length-scale-average gradient $\langle g_x \rangle$ is large, that is, if the gradient persists across length scales, then it is probably a feature edge and the diffusion is small. On the other hand, if the deviation, $\langle g_x^2 \rangle - \langle g_x \rangle^2$ is large, then the gradients do not persists across length scales, and the diffusion is large. The diffusion tensor will be nearly diagonal in a coordinate system that has one coordinate aligned with the local feature edge and one coordinate that is normal to the local feature edge, and so the anisotropic formulation has the virtue that it is capable of smoothing along edges while, at the same time, preserving the edge's position and steepness.

In Figure 3, we show the result of twenty iterations of this type of diffusion, which we call context-sensitive diffusion. The top left panel in Figure 3 shows a perspective view of the elevation after a 3x3 median filter, the top right panel shows the result of a Gaussian filter of width five pixels, the bottom left shows the result of context sensitive diffusion, and the bottom right shows the elevation that is manually derived from optical data. Note that the back and side edges of the context-sensitively diffused IFSAR elevation are about as sharp as in the median filtered elevation, but that the noise is reduced substantially.

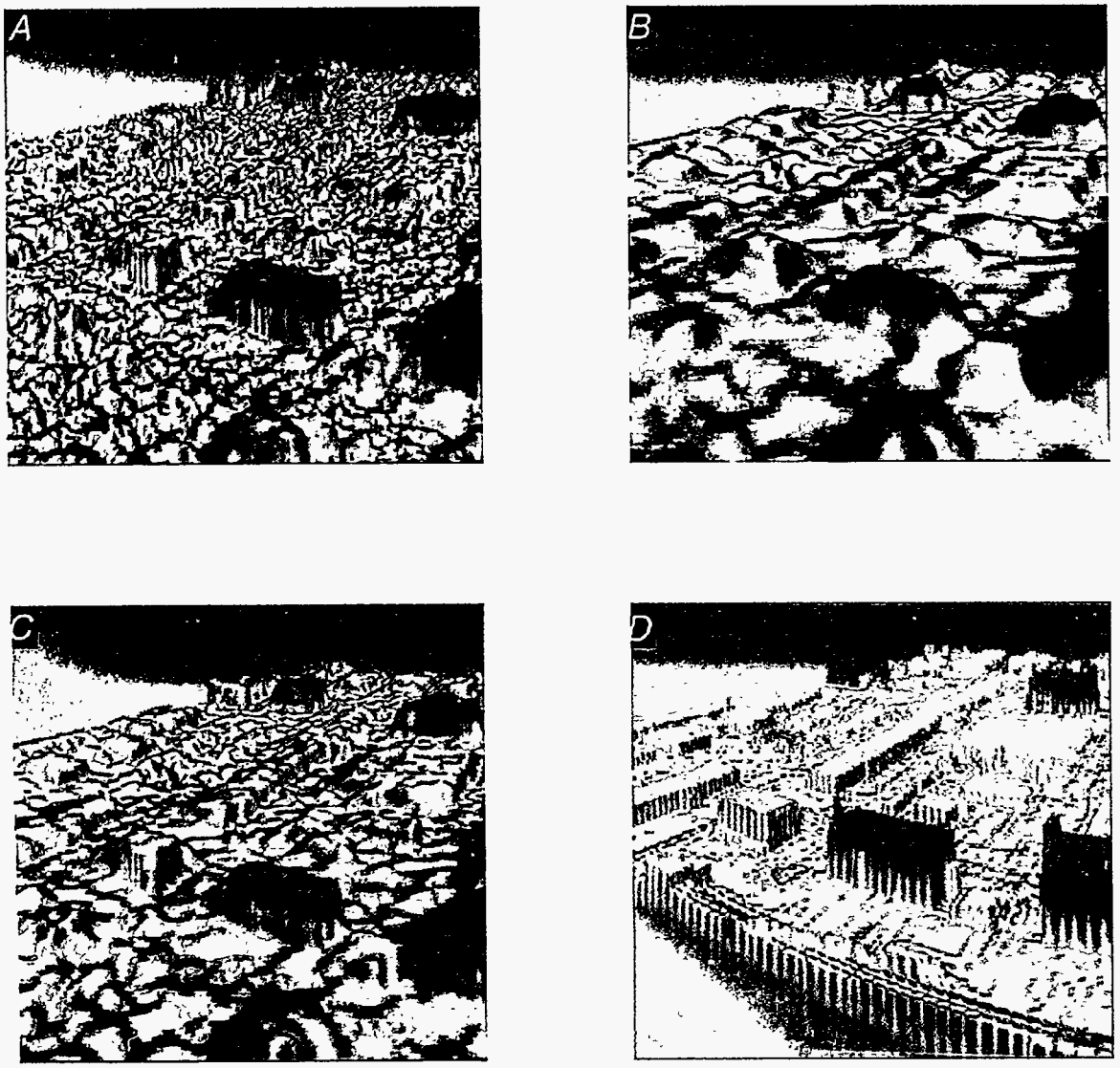

Figure 3: Comparison between A) the raw IFSAR elevation, B) Gaussian smoothed IFSAR elevation, C) context-sensitively diffused IFSAR elevation and D) the manually derived elevation.

4.2. *Front Porch Removal*

In Figure 4, we show an example of a building with a prominent "front porch" anomaly. This effect appears as an extended region on the near-range side of the building that is characterized by elevations in between the elevation at the ground and the elevation at the building top.

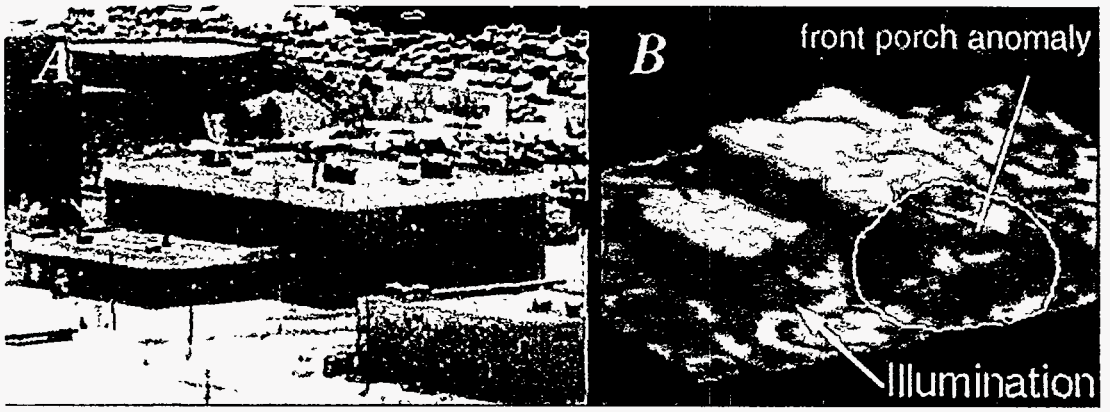

Figure 4: A) Perspective optical view of a building in the B894 scene, and B) a perspective view of the IFSAR elevation for the same building. The sloped region in front of the building in the IFSAR elevation is due to the front porch effect.

In Figure 5, we show a schematic drawing of a possible radar geometry for construction of elevation. Five different ranges are shown. The range R_1 only intersects the ground, so the IFSAR elevation measured for R_1 will be the elevation of the ground. For ranges $R_2 - R_4$, on the other hand, the radar will receive returns from both the ground and the building top. The elevation measured from these ranges will be an intensity weighted average of the ground elevation and the elevation of the building top. If the ground is much brighter than the building top, the elevation measured will be closer to the ground elevation, and vice versa. R_2 is the closest range that will give a mixed elevation, while R_4 is the farthest. Generally the corner at the base of the building is bright so that the elevation measured at R_4 will be closer to the ground elevation than for R_2 or R_3. For R_5 returns will come from the top of the building only, and so the elevation will be that of the top of the building.

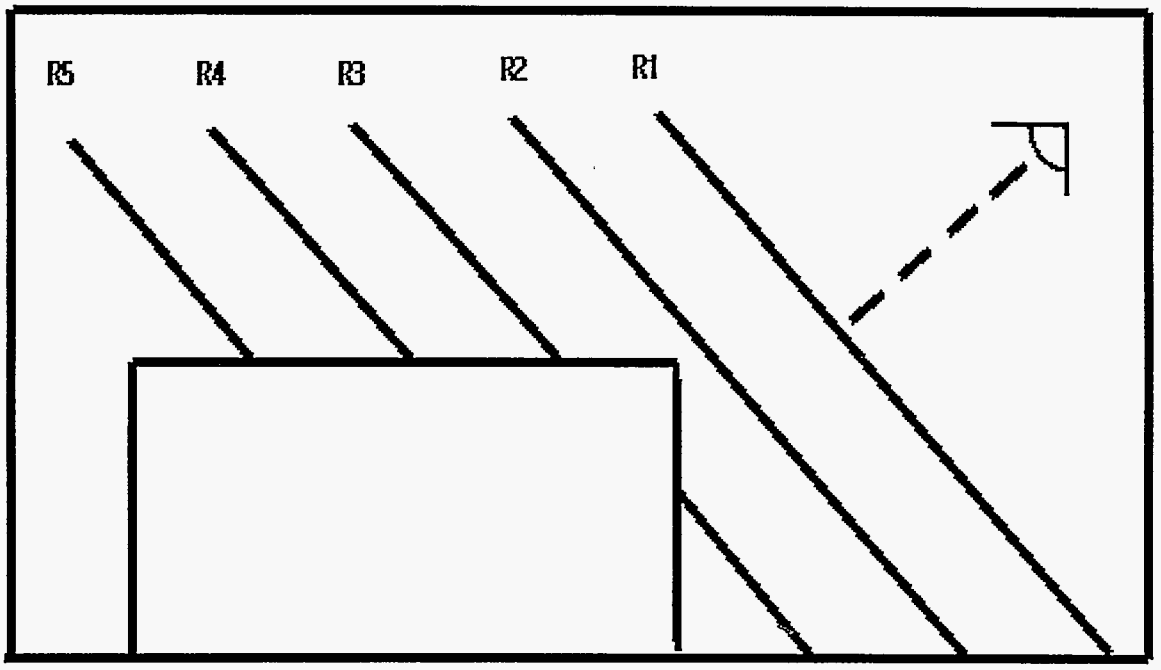

Figure 5: Schematic of an example radar geometry showing five different range possibilities.

Because the elevations measured at ranges R_2 -- R_4 are incorrect, during rectification they will be placed at incorrect ground distance y. The results of a simulation of the rectification for noiseless measurements are shown in Figure 6. In Figure 6a, we show the rectified elevation, in 6b we show the intensity, and in 6c we show the normalized binning number. For the simulation, five range measurements are placed into one bin on average. Starting at the near range, we first encounter ground measurements such as R_1 of Figure 5. Because the ground is assumed to be horizontal the binning number is average. The intensity is the backscatter intensity of the ground and the elevation is the ground elevation. At the rightmost green line, the region of the front port anomaly begins. The range intersecting the ground at this point is of the same type as R_2 above. Because this range gives a mixed elevation, the measurement is not placed at the "correct" position, but is instead misplaced to around $y = 17$. No measurements fall in between $y = 17$ and the rightmost green line, and so the binning number is small in that region. In reality, because of noise, some measurements will fall into this region and will have an elevation in between the ground elevation and the mixed elevation of the front porch. Measurements such as R_3 fall into the region $-10 < y < 17$, but the measurement that corresponds to R_4 is at the correct ground location because the corner reflector dominates. There then falls a second gap, followed by the correct placement of measurements such as R_5. The intensity measured in the front porch region is the geometric sum of the ground intensity and the building top intensity on average.

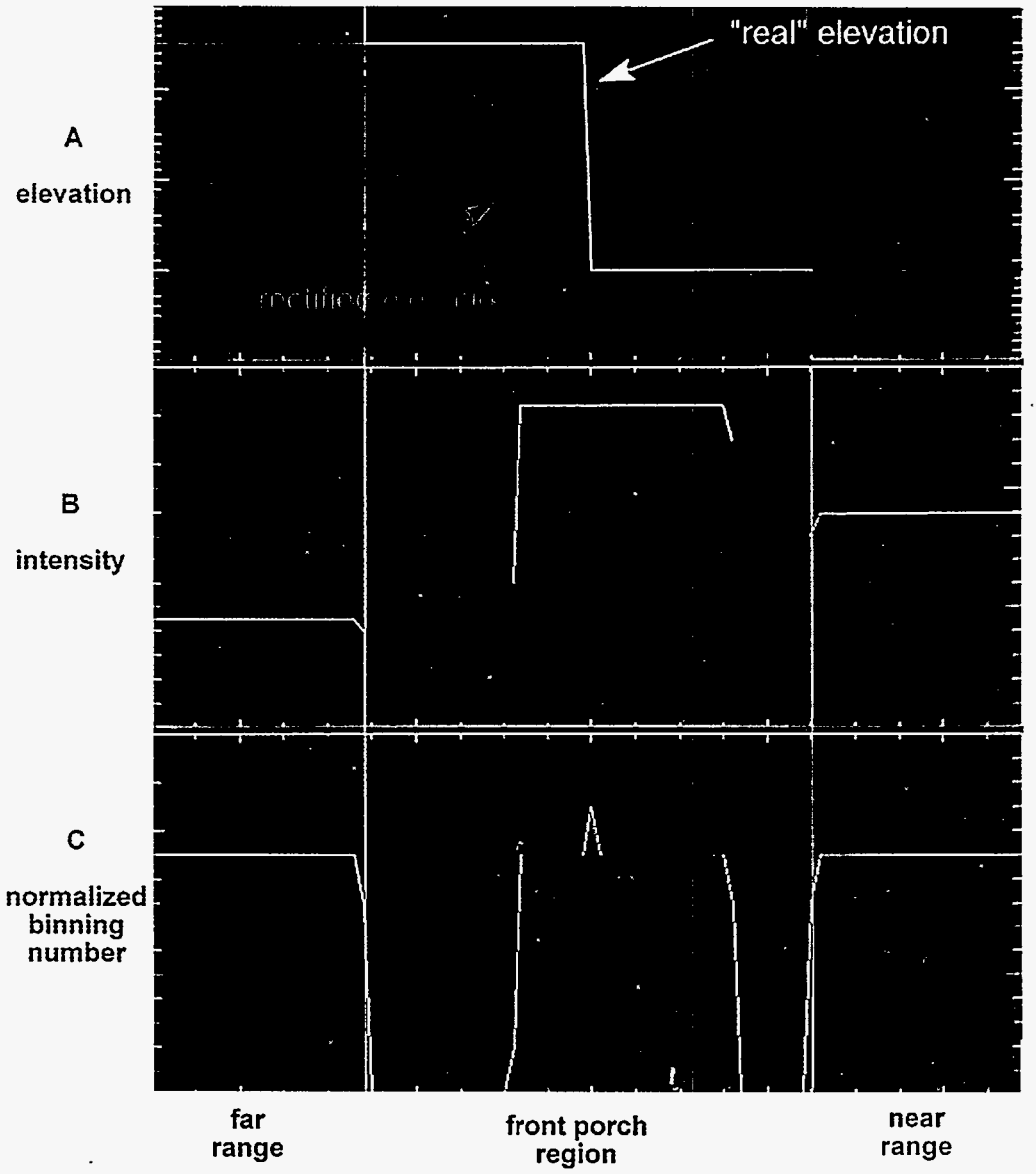

Figure 6: A front porch simulation showing (A) the actual (white) and expected (red) elevations, (B) the expected intensity, and (C) the expected normalized binning number.

One can easily see that the total length of the front porch region is $2\Delta h \tan i_0$, where i_0 is the nominal incidence angle to the ground in front of the building and Δh is the difference in height between the ground and the building top. The actual building edge is positioned midway between the front and the back of the front porch.

A cut of the same three parameters, elevation, intensity and normalized binning number, for the same building as was seen in Figure 4 is shown in Figure 7. We see, that as predicted, the front porch region is characterized by intermediate elevation and enhanced intensity, and it begins and is terminated by anomalously low binning numbers. Since the nominal incidence angle is about 45°, we expect that the length of the front porch will be approximately $2\Delta h$. In the case of Figure 7, $\Delta h \approx 13\text{m}$ and the length of the front porch is about 26m.

Identification of Front Porch Anomalies

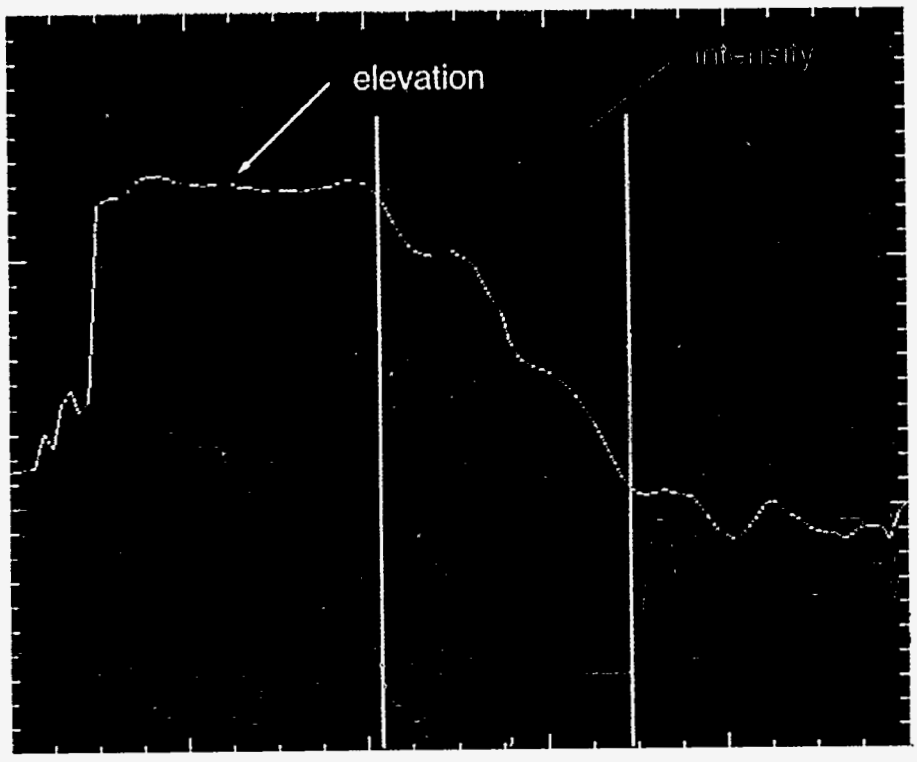

Figure 7: Cuts in the parameters taken across an actual front porch. Parameters shown are (white) the elevation, (red) the backscattered intensity, (blue) the binning number.

We use the above results to identify and correct for front porch regions, however, it should be noted that in the process, any actual features in the front porch region (such as real front porches!) are lost. In Figure 8, we show a comparison between perspective views of the context-sensitively smoothed elevation before and after front porch removal and the manually derived elevation. One can see that the front porch removal has improved the DEM significantly.

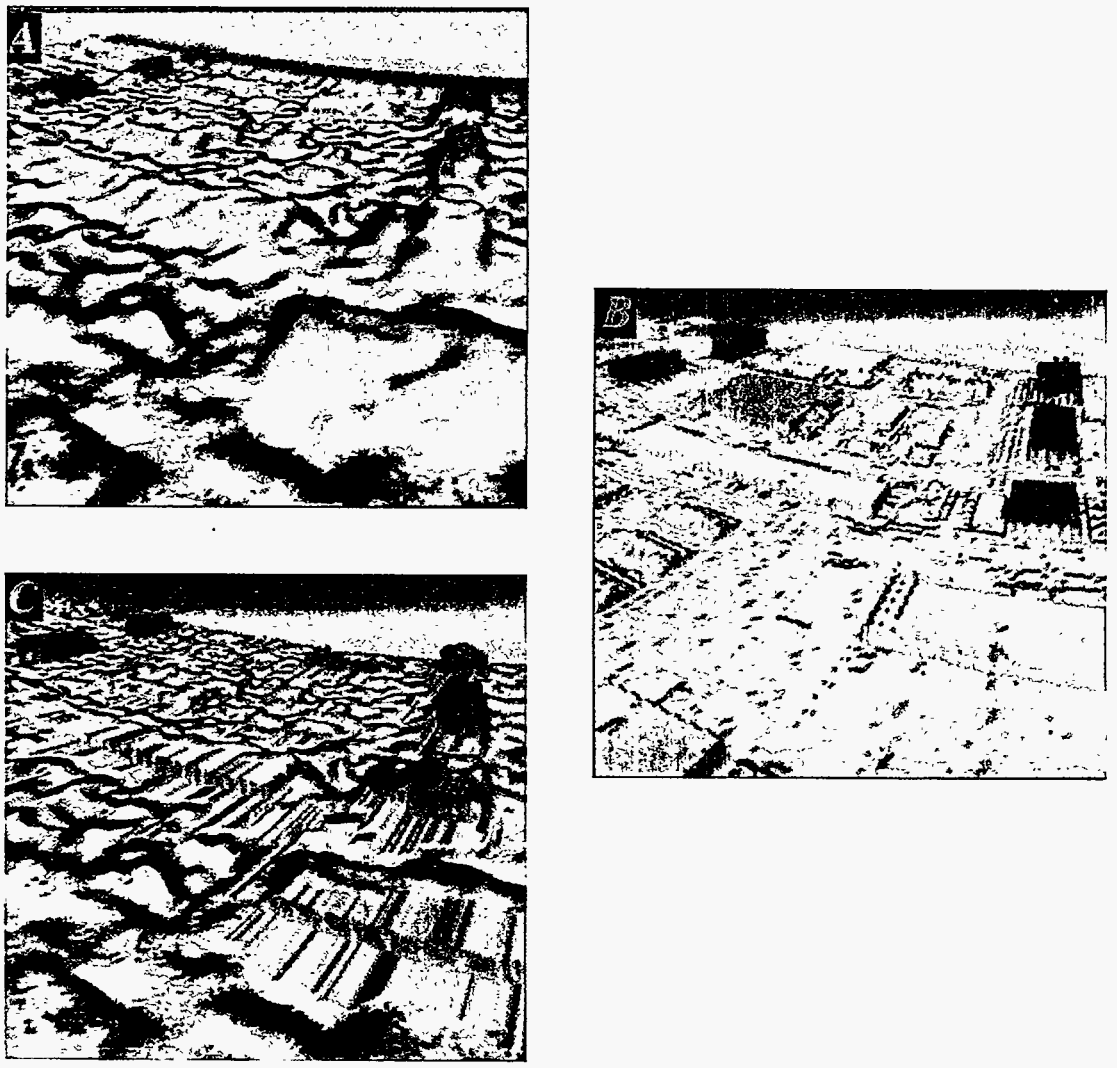

Figure 8: Comparison between the context sensitivity diffused IFSAR elevation (A) before and (C) after front porch removal, and (B) the manually derived elevation.

The comparison between the IFSAR elevation and the manually derived elevation is given in a more quantitative manner in Figure 9. Figure 9a shows the difference between the median filtered IFSAR elevation (3x3 median filtered) and the manually derived elevation, and 9b shows the difference between the IFSAR elevation that has been processed with context sensitive diffusion and front porch removal and the manually derived elevation. Figures 9a and 9b show the same building that was presented in Figure 7. The front edges of buildings in Figure 9a are characterized by first green, indicating that the IFSAR elevation is greater than the manually derived elevation, followed by red, indicating the opposite. First, considering the back and side edges of buildings, we see that the context-sensitive diffusion has substantially reduced the error that is due to thermal noise. Second, we see that the front porches have been successfully removed.

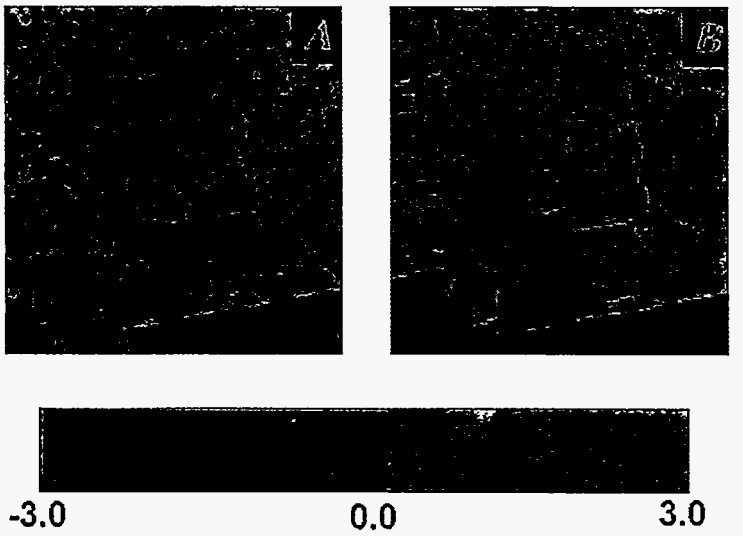

Figure 9: Quantitative result of DEM improvement. (A) The difference between the manually derived elevation and IFSAR elevation that has been filtered with a 3x3 median filter. (B) The difference between the manually derived elevation and the IFSAR elevation after context sensitive diffusion and front porch removal.

In Figure 10 we show the probability density function of the differences shown in Figure 9. The dashed line gives the probability density function of the differences of Figure 9a while the solid line gives the probability density function of the differences of Figure 9b. Although the manually derived DEM will have errors in it, the difference between the IFSAR elevation and the manually derived DEM is probably close to the error of the IFSAR DEM. Thus the dashed curve in Figure 10 represents the error of the original IFSAR DEM and the solid curve represents the error of the improved IFSAR DEM. We see that the diffusion and front porch removal has improved the accuracy of the DEM significantly, especially in the wings of the distribution. In conclusion, we find that the two processing techniques improve the IFSAR DEM significantly.

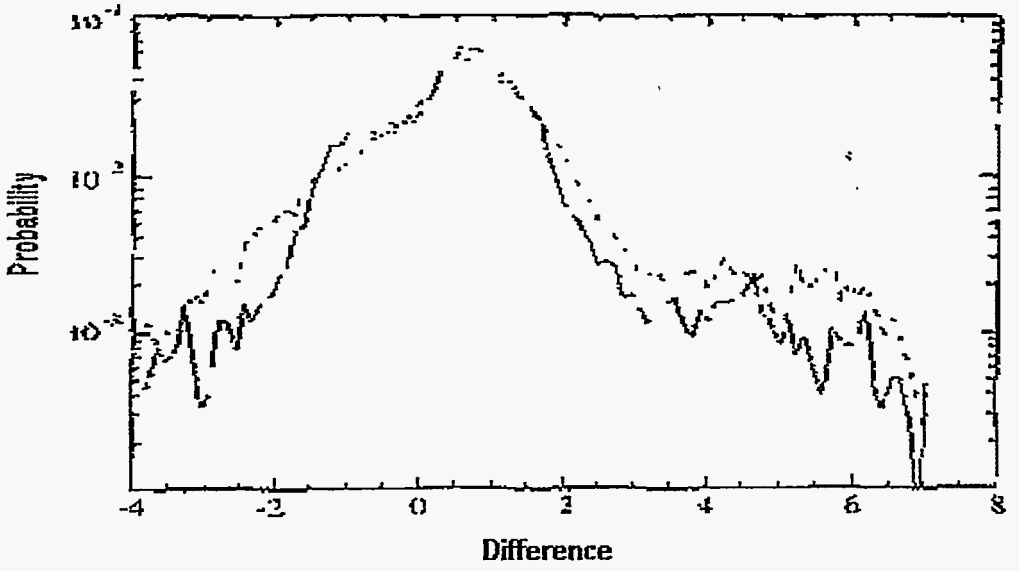

Figure 10: Probability density function of differences shown in Figure 9. The dashed line is the probability of the differences in Figure 9a while the solid line corresponds to Figure 9b.

5. Tree Extraction

In Figures 11 a, b, and c we show the "Infirmary" site. In Figure 11a, we show ortho-rectified optical data, while in Figures 11b and c we show the IFSAR backscatter intensity and elevation. Comparing the three images, we can identify trees in IFSAR data. Typically, trees are characterized by strong backscatter and high elevations.

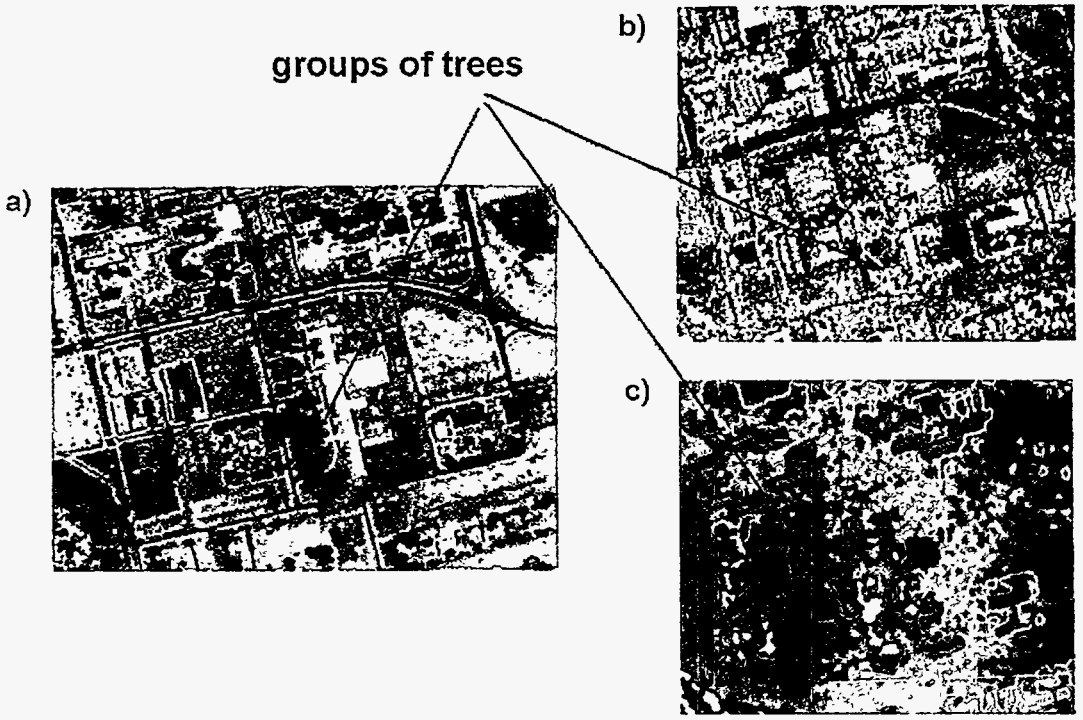

Figure 11: The Infirmary site which includes trees. (a) Optical data, (b) IFSAR backscatter intensity, (c) IFSAR elevation.

An additional indication of trees is the volume scattering decorrelation, δ_{vs}. This is the decorrelation that results from partial penetration into an object, and because trees are penetrable, it is suspected that the volume scattering decorrelation will be large for trees. To calculate the volume scattering decorrelation, we consider the correlation between the signals received by the two IFSAR antennas, $\rho = s_1 \bullet s_2 / |s_1||s_2|$. The decorrelation is related to the correlation by $\delta = 1 - \rho$. We separate the correlation into the different sources of decorrelation. These are: (1) the decorrelation resulting from thermal noise, δ_{th}; (2) the decorrelation due to a non-zero baseline, δ_{bl}.; (3) the decorrelation due to volume scattering δ_{vs}, and (4) decorrelation due to other sources, δ_o. Combining these together, we write,

$$\rho = \rho_{th}\rho_{vs}\rho_{bl}\rho_o$$

Assuming that we know the remaining sources of decorrelation, the volume scattering decorrelation can be found,

$$\delta_{vs} = 1 - \rho / \rho_{th}\rho_{vs}\rho_{bl}\rho_o$$

The baseline decorrelation is given by (Zebker and Villasenor [1992]),

$$\delta_{bl} = \left(\frac{2Br_g}{\lambda R}\right)\cos i$$

where B is the baseline, r_g is the ground resolution, R is the near range, λ is the wavelength and i is the incidence angle. We can calculate the incidence angle from the "binning number," N_1, or the number of looks that are placed into one pixel of the image. For purposes of the calculation above, however, ρ_{bl} need not be taken into account because it is very close to one.

The thermal decorrelation is, $\delta_{th} = 1 - \rho_{th}$, where

$\rho_{th} = SNR / (1 + SNR)$

and SNR is the signal-to-noise ratio.

If we assume that the decorrelation due to other sources is negligible, we may calculate the volume scattering decorrelation by

$\delta_{vs} = 1 - \rho / \rho_{th}$

At present we choose a value for the noise and calculate the volume decorrelation from the maximum correlation. (The maximum correlation is the greatest correlation for all the looks that are placed into one pixel of the image.) In Figures 12a-d, we show the optical image, the backscatter image, the maximum correlation and the volume scattering. We see that, indeed, the volume scattering decorrelation is large for many of the tree covered areas. It is also large, however, in some regions that are not tree covered. This is due to side-lobe contamination.

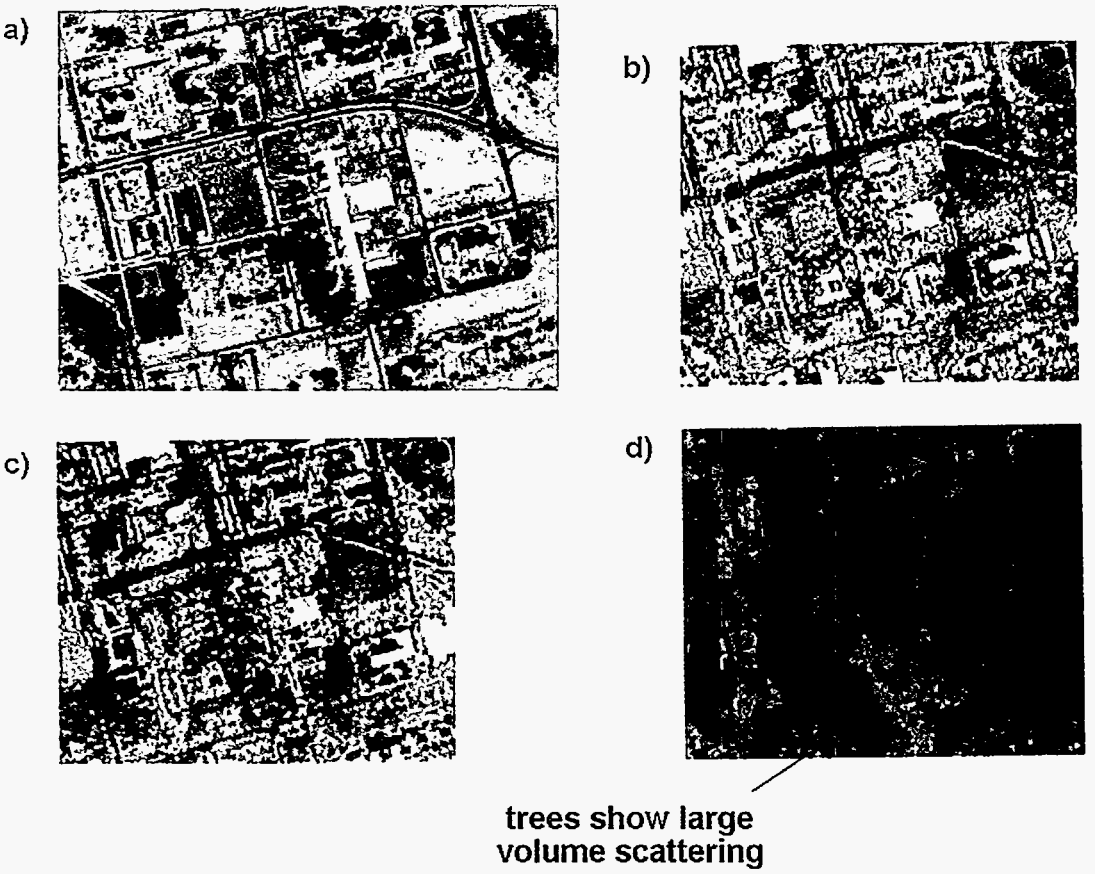

Figure 12: The Volume decorrelation. (a) Optical data, (b) IFSAR backscatter intensity (c) IFSAR maximum correlation, (d) volume scattering decorrelation.

6. Edge Detection

Assuming that trees are successfully extracted from the image, the next step is to identify the building edges. For this, we choose to principally use the elevation.

An oft quoted paper by Canny [1986] showed that on one dimension, an optimal edge detection algorithm takes the convolution of the derivative of a Gaussian function with the signal to be processed. Edges occur at maxima of the resulting function. The width of the Gaussian must be chosen to be larger than the typical scale length of the noise and smaller than the scale length of the features that are to be detected. Generally, inaccuracy in edge location increases with the width of the Gaussian.

In two dimensions, one must use the component of the gradient of the Gaussian that is directed normal to the edge one wishes to detect. It is possible to show, however that

$$\int_{-a}^{a} \frac{\partial g(x')}{\partial x'} h(x-x')dx' = \frac{\partial}{\partial x}\int_{-a}^{a} g(x')h(x-x^1)dx'$$

(assuming that g vanishes on boundaries placed at a and $-a$). We therefore can instead filter the image with a Gaussian and take for our edge function the magnitude of the gradient of the result.

For additional noise removal and better localization, we modify the procedure as follows:

We filter the data using a Gaussian of width equal to 3.5 pixels.

We calculate the gradients $g_N(x,y)_x = h(x+N,y) - h(x-N,y)$ and $g_N(x,y)_y = h(x,y+N) - h(x,y-N)$ for an initial length N where h is the elevation and the vector **g** is the gradient.

Where the magnitude of the gradient exceeds a given threshold, we reduce N by one-half and recalculate the gradients, repeating until N=5.

On the surviving pixels we calculated a sharpened gradient $g_s(x,y)_x = -h(x=2,y) + 3h(x+1,y) - 3h(x-1,y) + h(x-2,y)$ (and similarly for $g_s(x,y)_x$) and record the magnitude of the resulting gradient, $g = \left(g_{sx}^2 + g_{sy}^2\right)^{1/2}$.

The focusing portion of the procedure, steps 2 and 3, helps eliminate gradients due to noise in smooth regions. The smaller width Gaussian that this allows combined with the sharpening of step 4 results in better localization of the edge. The result of steps 1-4 is shown in Figure 13 for the "b-894" site.

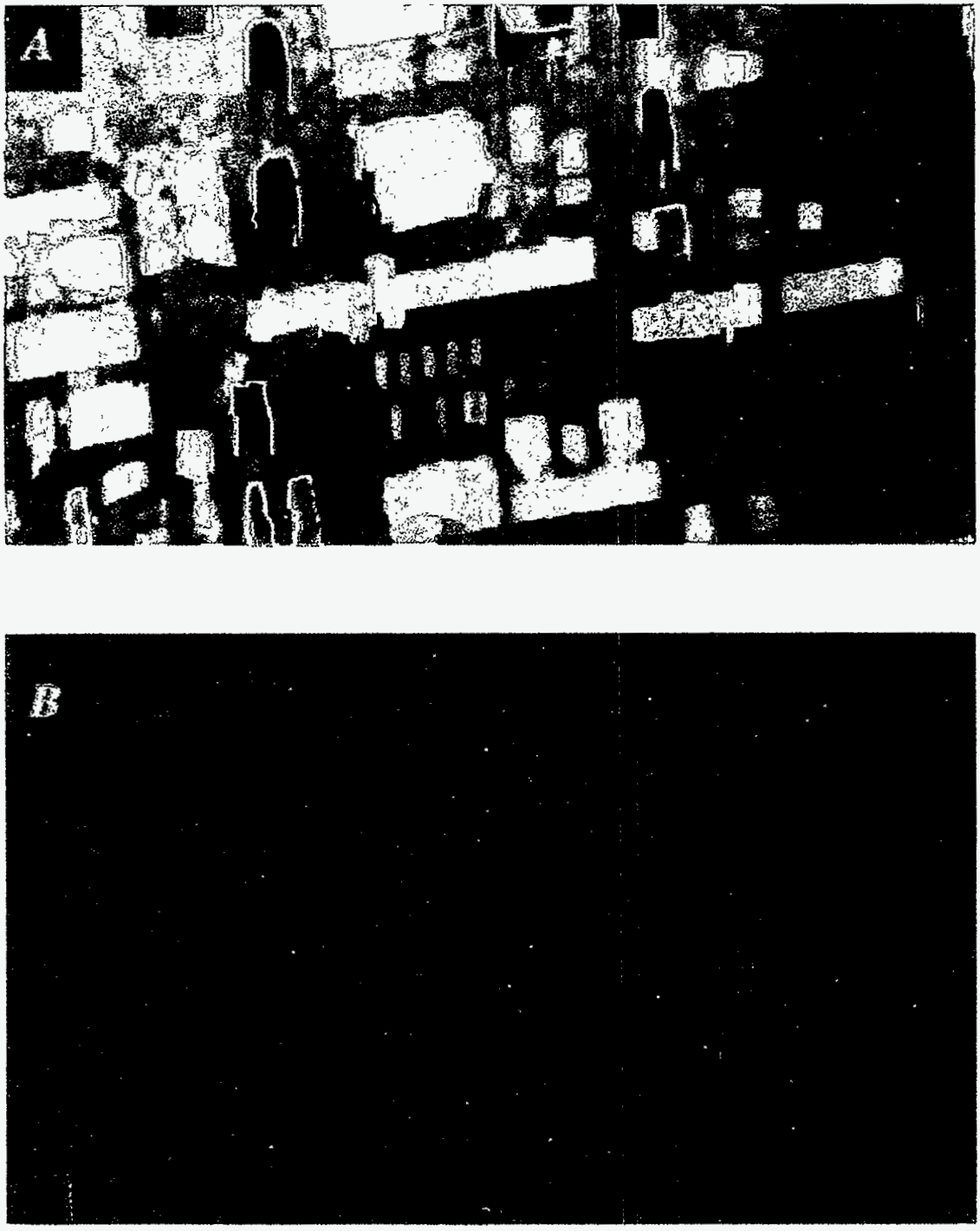

Figure 13: Gradient calculation. (A) The diffused elevation with shadows and front porches removed and (B) the gradient resulting from steps 1-4 above.

We then need to find vectors along lines of enhanced gradient. For this, we calculate the matrix $M = \begin{pmatrix} g_{xx} & g_{xy} \\ g_{yx} & g_{yy} \end{pmatrix}$, where $g_{xx} = 2g(x,y) - g(x+N,y) - g(x-N,y)$,

$g_{yy} = 2g(x,y) - g(x,y+N) - g(x,y-N)$, *and*

$g_{xy} = g_{yx} = \left[g(x+N,y+N) + g(x-N,y+N)\right]/2 - \left[g(x+N,y-N) + g(x-N,y-N)\right]/2$ where is the magnitude of the gradient as calculated above, and $N = 5$ is typically used. The unit eigenvector η that corresponds to the minimum eigenvalue of M is the direction along the edge, while the eigenvector ξ that corresponds to the maximum eigenvalue of M is the direction normal to the edge. To extract vectors that lie along edges, we first find points that are local maxima along ξ and then we connect the maxima along the direction η .

Figure 14: Comparison between IFSAR data and edge vectors. (A) comparison to IFSAR elevation, (B) comparison to IFSAR backscatter.

In Figure 14, the comparison between the edge vectors, extracted as above, and the IFSAR elevation and the IFSAR backscatter intensity is shown. We see that in comparison to the IFSAR elevation, the edge vectors very faithfully lie along the principal changes in raw elevation. The building front edges, however, are often fragmented because of the "front-porch" effect. The edges in the backscatter intensity are usually quite close to the vectors and the shadows that accompany back edges often intrude inside of the vectors.

7. Building Formation

We now proceed toward organizing the edge segments into building. Figure 15 a-d illustrates the steps for extracting rudimentary building footprints from the raw vector data derived from the gradient of the DEM. Figure 15a shows the raw vector data. Note that not all of the vectors follow the general trend of the building edges due to the aforementioned effects of "front-porching" and utility structures along building edges. We are currently working on ways to enhance the continuity of edge segments, particularly along front edges where they are fragmented. The first step toward extracting primitive building shapes is to clean the raw edge segments, join segments together, and eliminate overwritten edge segments. Figure 15b shows the results of cleaning the raw vector data. The second step (Figure 15c) is to decimate the edge segments by eliminating unnecessary vertices, eliminate edge segments that are small, and determine trend lines through least-squares fitting. The resulting edge segments are searched for branch points and divided at those points into separate segments. Finding the branch points within segments is necessary because the algorithm that searches for building corners uses intersections of disjoint segments. The third step is to form the edge segments into polygons (Figure 15d). Once the polygons are found, we can subtract the buildings from the DEM and form building models.

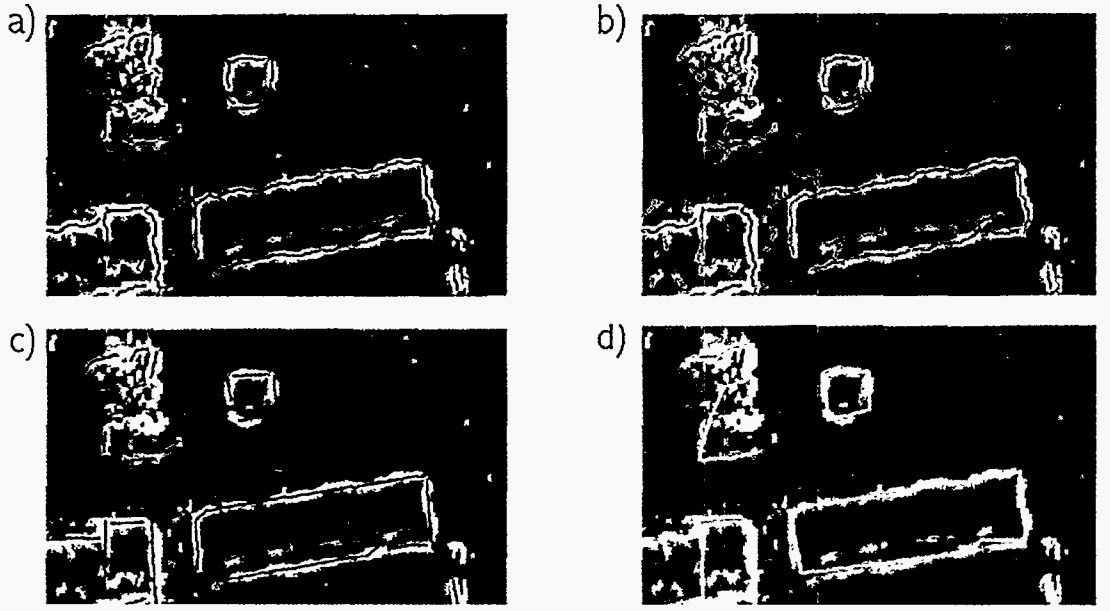

Figure 15: Simplification/Completion of edges. (A) Raw vectors, (B) cleaned vectors, (C) decimated vectors, (D) formation of polygons.

8. CAD Implementation

The process flow for translating the terrain and building information into a form suitable for input into the MicroStation CAD program is shown in Fig. 16. The files necessary for using the translator are the DEM file and the ASCII building file. Future implementations of the application may include inputs for other features such as trees or other structures of interest. The application that runs within the MicroStation environment is called BuildM. BuildM is a program written in MDL which is a language that has access to the CAD functionality inherent in MicroStation. BuildM runs seamlessly within MicroStation.

Refer to Fig. 16 for the following description. The DEM file requires some pre-processing before input into BuildM. A C program (bin2ascii) accomplishes this by reading the binary DEM file and writing out an ASCII version that BuildM can read. The building file contains the building perimeter description, building height, and base elevation of each building. These two files are read by BuildM into the MicroStation environment as design elements in a design file. Once in the design file, these elements can be edited like any other design file elements. A design file is similar to a CGM or other graphics file but contains 3D information. Internally, the MDL language allows direct access to the elements in the design file.

The BuildM application allows the user to input the DEM and buildings on separate "levels". A level is analogous to a layer in a GIS where mutually exclusive processes can be run on each level without affecting another feature on a different level. Levels are useful for viewing also. By turning on/off certain levels it is possible to display only those feature of interest. A user might want to view the buildings alone without the DEM for editing for example.

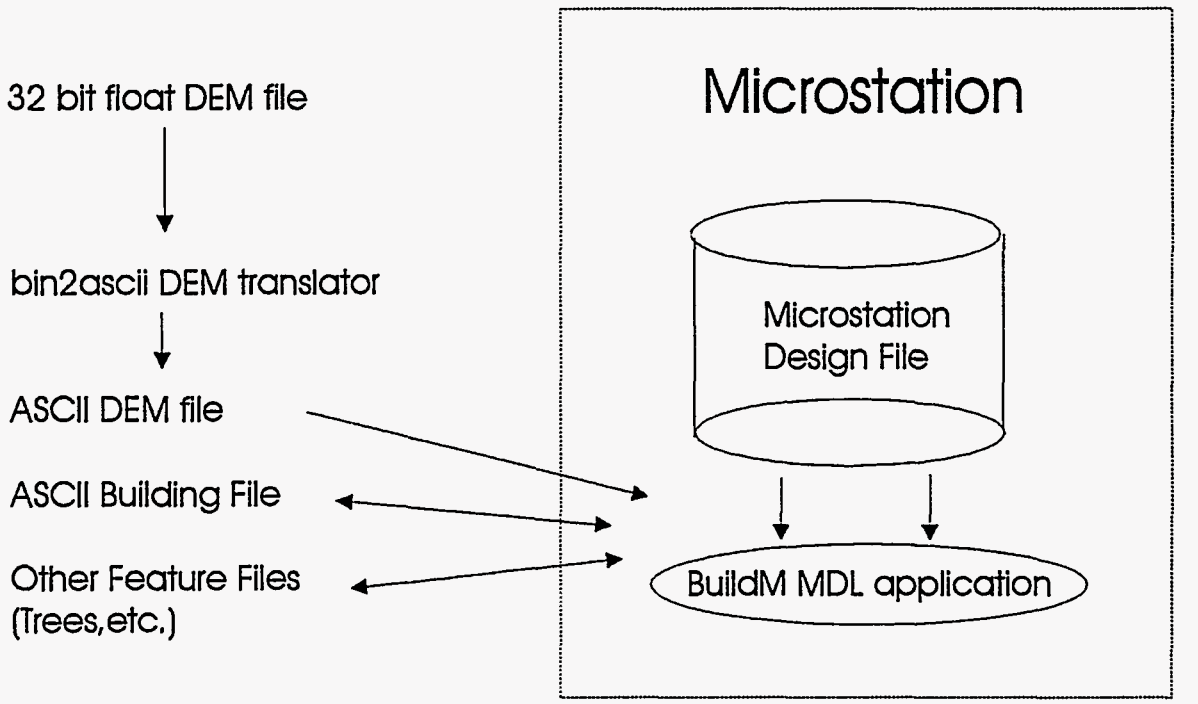

Figure 16: Schematic for processing building output for input into MicroStation.

8.0 Summary

8.1. Results

Vexcel's method for DEM reconstruction exploiting previously unused radar information achieves very good results by using a four-phase approach. First, they detect and segment the elevation model into four "classes" of data. The classes are:

- Shadows (Noise)
- Buildings
- Trees
- "Bald Earth"

Second, they apply an iterative algorithm to fill shadow areas with a height estimated from the surrounding area. Next, they apply various algorithms to clean up the areas which have buildings. These areas include the building itself and the layover (or front-porch area) in front of the building. This work is done from the building data in conjunction with the estimated "Bald Earth" map in the area immediately surrounding the building. Finally, the algorithm recombines the trees, the buildings, and the filled-in shadows with the original model to produce a complete model, including the new estimated data.

8.2. *Future Work*

There are several other ways to approach the solution for multiple objects with disparate heights occupying the same range-doppler cell.

- Assume that there are no more than two objects in the cell and mathematically solve for their positions using estimates of each object's radar cross section (or some other parameter).
- Use more observations – either more than two antennas, or multiple passes of IFSAR, or IFSAR from multiple directions.

Both of these approaches potentially use more of the information available from the IFSAR to predict the correct solution. They will probably lead to solutions which are even more robust – that is, they will yield the correct answer in more situations.

9. References

Bickel & Hensley, Design, Theory, and Applications of Interferometric Synthetic Aperture Radar for Topographic Mapping, SAND96-1092

Canny, J., A computational approach to edge detection, *IEEE Transactions on Pattern Analysis and Machine Intelligence*, **PAMI-8**, 679, 1986.

Zebker, H. A., and J. Villasenor, Decorrelation in Interferometric Radar Echoes, *IEEE Transactions on Geoscience and Remote Sensing*, **30**, 950, 1992

Distribution:

1	0529	B. C. Walker, 2345
1	0537	R. M. Axline, 2344
1	0537	D. L. Bickel, 2344
5	0537	W. H. Hensley, 2344
1	0537	J. T. Cordaro, 2344
1	0572	T. S. Prevender, 5912
15	0843	J. R. Fellerhoff, 2525
1	0843	J. D. Bradley, 2525
1	0843	J. R. Ellis, 2525
1	0859	R. M. Huelskamp, 2527
3	0161	Patent & Licensing Office, 1150
1	9018	Central Technical Files, 8940-2
5	0899	Technical Library, 4414
2	0619	Review & Approval Desk, For DOE/OSTI